lian Journal of Engineering Geology and Environm
www.ijege.uniroma1.it

# ASSESSMENT OF THE MECHANISM OF EXCESSIVE DEFORMATIONS ENCOUNTERED IN A LARGE-SPAN TUNNEL EXCAVATION USING ANALYTICAL AND 3D NUMERICAL ANALYSES

Ebu Bekir AYGAR(*) & Candan GOKCEOGLU(**)

*(*)Fugro Geosciences Consulting Engineering Ltd - 06680 Cankaya, Ankara (Turkey)*
*(**)Hacettepe University, Geological Engineering Department - 06800 Ankara (Turkey)*
*Corresponding author: cgokce@hacettepe.edu.tr; candan.gokceoglu@gmail.com*

## EXTENDED ABSTRACT

Il tunnel T8 (L=3826 m) si trova nella sezione Dogancay nel progetto ferroviario ad alta velocità Ankara-İstanbul. Il tunnel è stato progettato e scavato con il Nuovo Metodo Austriaco di Tunnelling (NATM) attraversando diverse unità litologiche costituite da graniti, calcari e scisti argillosi. Inoltre, parte del percorso della galleria tra i km:142+280 - 142+360 è interessata da frane di cui si è dovuto tener conto nella progettazione anche se a causa dei vincoli geometrici della ferrovia ad alta velocità, è stato necessario attraversare frane o zone limitrofe. Nell'ambito di tale progetto, il tunnel T8, la cui costruzione è stata completata ad Adapazarı, sezione Doğançay, è stato scavato in aree in frana e a seguito delle indagini geotecniche, comprensive di prove in foro e in situ, l'altezza della calotta del tunnel è stata progettata per essere 10 m al di sotto della superficie di rottura della frana. Durante lo scavo in questa zona del tunnel si sono verificate deformazioni eccessive che in alcuni punti hanno superato la tolleranza massima di 15 cm. Tuttavia, la stabilità del tunnel è stata raggiunta con miglioramenti e supporti aggiuntivi.

Lo scopo del presente studio è quello di indagare le eccessive deformazioni avvenute durante la fase di scavo e di comprendere l'effetto della frana su tali deformazioni mediante analisi analitiche e numeriche 3D, studiando, inoltre, l'interazione tra galleria e frana e i sistemi di supporto per questo tipo di problemi.

Lungo il percorso del tunnel T8, sono state incontrate due diverse unità litologiche. A circa km:139+253 dall'imbocco del tunnel, è attraversato il nucleo granitico della formazione Abant, generalmente da moderatamente a leggermente alterata e fratturata. La restante parte del percorso è stata scavata nei membri calcarei, marnosi e scistosi della stessa Formazione, separata dall'unità granitica da un contatto tettonico costituito da una faglia trascorrente. Le unità circostanti solitamente contengono acque sotterranee intrappolate poiché sono impermeabili. Lungo il percorso sono presenti alcune frane tra i km: 139+221 - 140+857 e la profondità della superficie di rottura delle frane varia tra 19 e 56 m. Inoltre, tra i km:142+000 - 142+480 il tunnel passa interamente in zona di faglia e a causa delle frane e dello scarso spessore del materiale di copertura, in questa sezione della galleria non si sono formati archi. Inoltre, a seconda delle proprietà di rigonfiamento e compressione a lungo termine delle unità argillose, in questa sezione sono aumentati i carichi sui supporti e si sono verificati cedimenti, osservando durante lo scavo gravi deformazioni nella galleria dovute a tali condizioni avverse.

Tuttavia, poichè in questo caso la superficie di rottura non taglia la galleria, non esiste un'interazione diretta tra frana e galleria. Pertanto sono stati studiati i dettagli dell'interazione indiretta attraverso l'esecuzione di analisi numeriche 3D, i cui risultati hanno mostrato coerenza con quelli delle misurazioni in situ. Il completamento dell'anello di rivestimento durante lo scavo di un tunnel è stato molto importante per la sua stabilità e una delle conclusioni più importanti ottenute dallo studio è che la distanza tra la galleria e la superficie di rottura della frana non dovrebbe essere inferiore a 10 m nelle gallerie da scavare sotto aree in frane. Infatti, sia nelle misurazioni di sito che nell'analisi numerica si è osservato che l'effetto franoso indiretto dello scavo del tunnel esiste ma è limitato tanto che il tunnel T8 è stato costruito con successo, aperto al traffico e non sono stati riscontrati problemi.

Le deformazioni eccessive avvenute nel tunnel generalmente terminavano a una distanza 2D e la chiusura dell'anello di rivestimento a tale distanza su terreni deboli influisce positivamente sulla stabilità del tunnel. La principale fonte delle deformazioni e dei cedimenti nel tunnel è dovuta alle elevate pressioni orizzontali, e questo è l'effetto negativo indiretto del materiale di frana in superficie. Tuttavia, nonostante le deformazioni, la stabilità del tunnel è stata garantita grazie alla riprofilatura e ai lavori di sostegno aggiuntivi. La progettazione del sistema di supporto del tunnel dovrebbe essere rigida per ridurre al minimo le deformazioni in condizioni di rigonfiamento e nella zona di frana.

In definitiva, i risultati del presente studio possono fornire una base scientifica per la progettazione ottimale dei supporti nella costruzione di gallerie in aree in frana.

*IJEGE, 1 (2024): 17-33, DOI: 10.4408/IJEGE.2024-01.O-02*
*E-ISSN 2035-5688 | ISSN 1825-6635 / ©Author(s)*

## ABSTRACT

T8 tunnel (L=3826 m) is located in Dogancay Section in Ankara-İstanbul High Speed Railway Project. The tunnel was designed and excavated with New Austrian Tunnelling Method (NATM). The tunnel route was composed of granite, mudstone, and shale units. A part of the tunnel route between km:142+280 - 142+360 contains landslides. While determining the tunnel route, it is desirable to avoid landslides as much as possible. However, due to the geometrical restrictions of a high-speed railway, it is necessary to pass through the landslide or parts close to the landslide. As part of the Ankara-Istanbul High-Speed Railway Project, the T8 tunnel, the construction of which was completed in Adapazarı, Doğançay section, was excavated under landslides. As a result of the geotechnical investigations including borehole and in-situ tests, the tunnel roof altitude was designed to be 10 m below the failure surface of the landslide. During the excavation in this region in the tunnel, excessive deformations occurred in places that exceeded the maximum deformation tolerance of 15 cm. However, tunnel stability was achieved with improvements and additional support. The purposes of the study are to explain the excessive deformations that occurred during the excavation stage and to understand the effect of the landslide on these deformations using analytical and 3D numerical analyses. Within the purpose of the study, the relationship between a tunnel and a landslide is investigated, and support systems for these types of problems are described. The results showed that the main source of the excessive deformations and failures in the tunnel is due to the high horizontal pressures caused by the landslide material on the surface.

Consequently, the results of the study may provide a scientific basis for the optimum support design of tunnel construction under landslides.


***Keywords****: landslide, high-speed railway, tunnel support system, weak ground*

## INTRODUCTION

Especially, the high-speed railways have several geometrical limitations such as high curve radius and low longitudinal slope. This situation directly affects construction costs. The parameters used for optimum railway route selection are cost, allowable speed, length of route, number of stations and accessibility, amount of long tunnel, amount of high viaduct, and amount of displacement of the existing conventional railway (Gokceoglu *et alii*, 2014). Tunnels are the important parts of high-speed railway projects and, one of the most important stages during tunnel design is the most suitable route selection. However, the tunnel route is not independent of the whole railway route. While choosing the route, landslide areas are tried to be avoided due to the adverse effect of landslides on tunnel construction. As stated, in High-Speed Railway projects, it is not always possible to avoid landslide areas from time to time due to the dependency on the whole project route. In these cases, tunnel and portal sections must be designed considering the adverse effects of landslides. During tunnel excavation, a rigid support system during excavations is generally chosen, and deformation is not allowed under landslides. Aygar & Gokceoglu (2021) investigated the problems experienced due to landslide problems in the portal section of the Geminbeli tunnel and emphasized that a rigid support system is required by constructing a cut-and-cover structure in the portal section. During the Ankara-İstanbul high-speed railway construction, several landslides occurred and, some of these problems affected the portals and tunnels. A typical example of the adverse landslide effects on the portal and tunnel is T26 tunnel. The landslide at the T26 tunnel entrance portal was investigated, the geometry of the landslide body and failure surface was determined, and the tunnel route had to be shifted towards the mountain part to avoid interaction with the landslide (Aygar & Gokceoglu, 2019). Subsequently, Gokceoglu *et alii*, (2022) described the geotechnical problems encountered during the T26 tunnel construction, and one of these problems was landslides. Vlachopoulos *et alii* (2015) performed analytical and numerical analyzes examined to understand tunnel behavior in weak rocks. Xiao *et alii* (2014) investigated the mechanisms of cracks occurring in secondary linings in tunnels subjected to asymmetric loading in low overburden and loose soils and they stated that the impact of the construction stages on the secondary lining is serious. Kim *et alii* (2020) examined the long-term deformations in the tunnel near fault zone. In order to prevent swelling in the invert, Kim *et alii* (2020) suggested the injection method to strengthen the invert. Manasa & Maji (2023) numerically investigated the effect of different tunnel shapes in squeezed rocks. In this study, numerical analyzes were carried out with the *Flac v7.0* program using circular, inverted-D and horseshoe type sections. Manasa & Maji (2023) employed different overburden heights and different GSI values in the analyses. Shrestha & Panthi (2014) stated that deformations increased by 30% when the groundwater pressure was up to 1.5 bar. Xiao *et alii* (2016) examined the effects of different tunnel excavation stages in loose soil on tunnel stability and they revealed that stresses were high in secondary linings after completion of tunnel excavation in loose soils. Gattinoni *et alii* (2019) investigated the relationship between the tunnel excavated under an active shallow landslide and the landslide during excavation. According to Gattinoni *et alii* (2019), water coming from cracks in weak ground causes undesirable time losses and cost increases in the tunnel.

Zhang *et alii* (2017) stated in their study that the tunnel

excavation technique is very important in terms of tunnel and landslide stability. Lunardi *et alii* (2017) emphasized the importance of tunnel route planning and examined the relationship between landslide and tunnel by 3D numerical analysis in different tunnels. Ruggeri *et alii* (2016), on the other hand, studied the triggering mechanism of a landslide during tunnel excavation and focused on a solution proposal consisting of the deep drainage system, and long radial drainage pipes. Wu & Pail (2020) surveyed the tunnel landslide relationship and the change in the factor of safety in the Guo-Jia tunnel with the help of 3D numerical analysis. They determined that the factor of safety of the landslide in the Guo-Jia tunnel, which was excavated as a double tube and has a maximum overburden height of 140 m, also in their study vertical distance from the tunnel roof to the surface greater than 10 m, safety factor did not change. Ayoublou *et alii* (2019) investigated the impact of a landslide on the portal section of the Sabzkuh tunnel which is 10.617 m long. They emphasized that failures occurred in the tunnel due to the deformations that developed as a consequence of the tunnel excavation method. Depending on the experienced problems, they focused on the engineering solution proposals for re-excavation of the tunnel and ensuring the stability of the portal.

Zhang *et alii* (2021a) investigated the landslide mechanism at the railway tunnel portal of in Chinese railway which passes poorly geological conditions. In the paper of Zhang *et alii* (2021a), based on a railway, the mechanism of landslide-tunnel interaction is investigated employing long-term monitoring and numerical calculation. Zhijie *et alii* (2020), on the other hand, examined the effect of landslide on the tunnel lining to reveal the internal force law of tunnel structure on different positions of landslide tunnel system with numerical analyses and stated that the cross-sectional effects increased with the landslide effect. Zhang *et alii* (2021b) assessed the displacements in the tunnel lining and tunnel portal slopes with 3D numerical analysis and emphasized that large portal slopes are critical. Xiang & Liu (2021) studied the relationship between landslide movement and deformation in the tunnel. Xiang & Liu (2021) employed numerical analysis to investigate the different excavation patterns affecting the stress and deformation of landslide crossed orthogonally by tunnel. Komu *et alii* (2020) studied the landslide relationship of the tunnel excavated in the Bahce-Nurdag project with 3D analysis and stated that the 600 m section of the tunnel is under the effect of landslide. This tunnel is located in the region affected by the 6 February 2023 Türkiye Earthquakes, but no damage occurred (Gokceoglu & Karahan, 2023). Zhou *et alii* (2020) investigated a loess-mudstone landslide and the induced structural damage in a high-speed railway tunnel with 2D numerical analyses. In addition, different researchers have conducted studies on the tunnel and landslide relationship such as Barla *et alii* (2015), Causse *et alii* (2015), Bandini *et alii* (2015), Hungr & McDougall (2009), Zhang *et alii* (2015 and 2017), Casusse *et alii* (2015), Huang & Xiao (2010), Zhu *et alii* (2021), and Wei *et alii* (2023).

The T8 tunnel was designed with the New Austrian Tunneling Method (NATM). As is known, NATM is based on the principle of maximizing the bearing capacity of the ground by allowing deformation around the tunnel (Rabcewicz 1964, 1965a and b; Rabcewicz & Golser, 1973; Muller, 1978). However, it was stated in NATM that revision is needed for the weak ground conditions (Aygar, 2000, 2007, and 2020). For this reason, it has been stated that a rigid support system is required instead of a flexible outer arch principle in the weak ground (Aygar, 2020). Although the T8 tunnel was basically designed with NATM, a rigid support system was used due to weak geotechnical conditions and adverse effects of landslides. Minglei *et alii* (2022) stated that "when the tunnel passes through the slope area, once the slope stability changes or landslide disasters occur, large additional stress, deformation, or cracking are easily caused in the tunnel, which results in high risk to the tunnel operation". When considering this statement, if a tunnel route passes through landslide zone, some extra efforts must be performed considering possible adverse effects of landslides. To explain the excessive deformations that occurred during the excavation stage of a large-span high-speed railway tunnel and to understand the effect of the landslide on these deformations using analytical and 3D numerical analyses are the purposes of the present study. The T8 tunnel construction is a complex landslide – tunnel interaction case, and a scientific basis for the tunnel construction in weak ground conditions and under landslide is presented. For the purpose of the study, the T8 tunnel case and its excessive deformations are evaluated with analytical and 3D numerical analyses, and the results are checked by employing in-situ measurements and observations during the tunnel construction. In fact, each tunnel case constructed in weak ground conditions, and under the adverse effects of other factors such as landslides, shallow conditions, and under highways or buildings is important and interesting for international tunneling, engineering geology, and rock mechanics communities. Consequently, the case presented in the study may be useful for the next tunnel constructions to be excavated in weak ground conditions and under landslides.

## GENERAL SPECIFICATIONS OF THE T8 TUNNEL

The T8 tunnel is between km:138+954 - 142+780 of the Ankara-Istanbul High-Speed Railway Project, and its total length is 3826 m (Fig. 1). The altitude of the tunnel entrance is 90 m, and the altitude of the exit portal decreases to 78 m. The

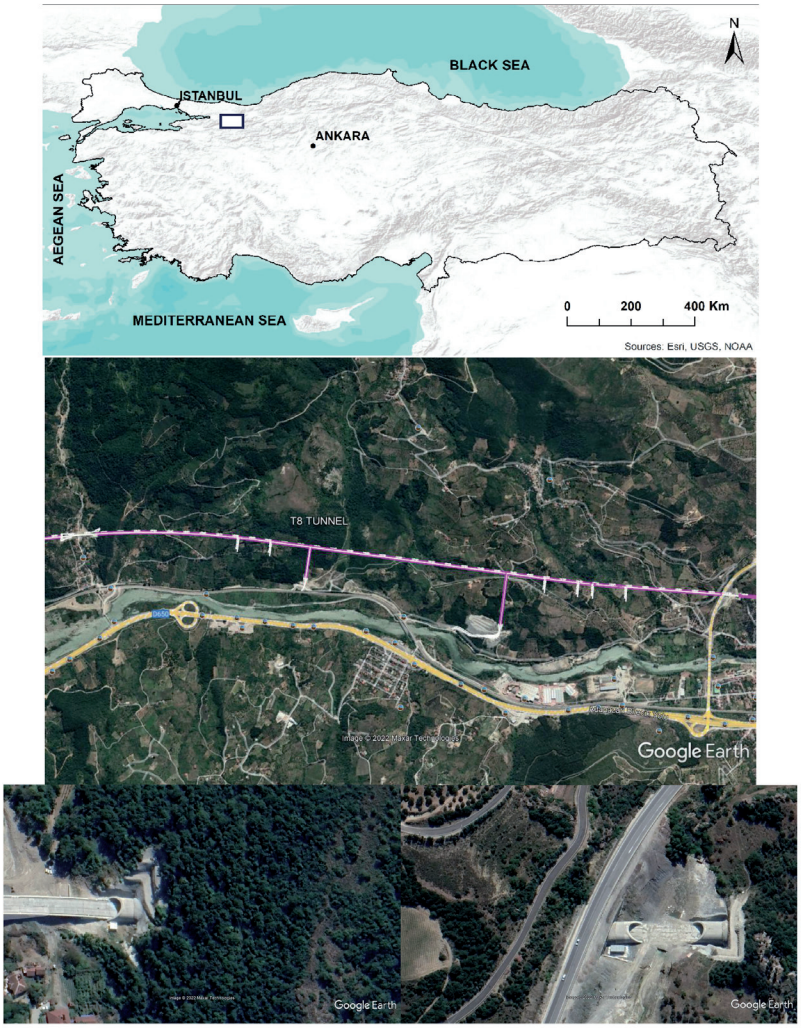


*Fig. 1 - Location map of the T8 tunnel and its entrance and exit portals on Google Earth images*

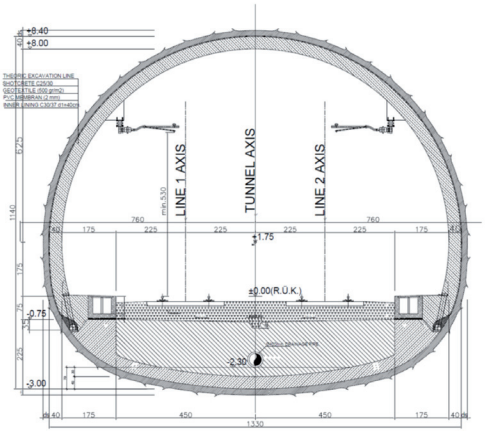


*Fig. 2 - Typical cross-section of the T8 tunnel*

thickness of the tunnel overburden varies between 6 and 150 m (Fugro Sial, 2009). The Google Earth image and plan of the tunnel route are depicted in Fig. 1. The height of the T8 tunnel, which is designed as a single tube, is 8.0 m and the excavation diameter is 13.5 m (Fig. 2).

## GEOLOGICAL AND GEOTECHNICAL CONDITIONS OF THE T8 TUNNEL ROUTE

Two different lithological units were encountered along the T8 tunnel route (Fig. 3). At approximately km:139+253 from the tunnel's entrance portal, te tunnel passes entirely through the granite unit of the Abant formation which Upper Campanian – Lower Eocene (Özer *et alii,* 2013). The unit is brown on the surface and gray in the depths and is generally moderately - slightly weathered and jointed. The remaining part of the T8

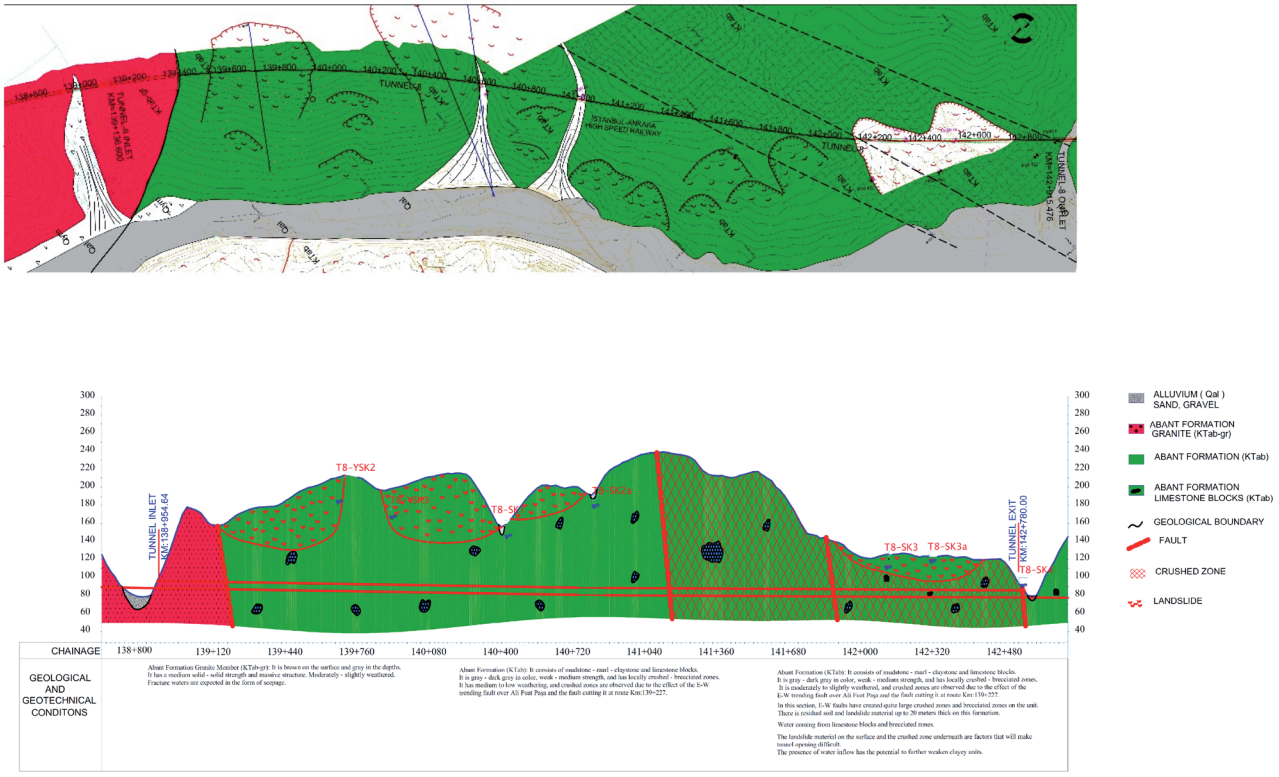


*Fig. 3 - Geological-geotechnical plan and profile of the T8 tunnel (Fugro Sial, 2009)*

tunnel route was excavated in the mudstone, marl, and shale members of the Abant Formation, which is separated from the Granite unit by a tectonic contact consisting of a strike-slip fault. The formation contains slightly weathered-fresh, and locally crushed zones. Between km: 139+258 and the exit portal (km: 142+778.48), the tunnel passes through the mudstone-claystone-marl alternation of the Abant Formation. There are brown-purple-red limestone tectonic blocks in the formation. These blocks range from a few decimetres to meters. Surrounding units usually contain perched groundwater as they are impermeable. There are some landslides between km: 139+221 - 140+857 along the route. The failure surface depths of the landslides in the soundings here vary between 19 and 56 m. It was observed that the units formed crushed zones due to the fault effect in the soundings in these intervals (T8-SK1, T8-SK2, T8-SK2A, T8-SK3 and T8-SK3A). Fault zones in NE-SW direction affected the tunnel route between approximately km: 141+226 and the exit portal. In this section, the fault clays, which turned into a residual soil feature due to the fault effect, lost their stability on the surface. According to the boreholes, the landslide depth is approximately 15 m (T8-SK3A) above the tunnel roof (Fugro Sial, 2009). It is evident that the tunnel-landslide interaction in this case is indirect because the distance between the tunnel roof and the failure surface is about 15 m.

### *Geotechnical parameters of exit portal section (km:141+940)*

To apply the analytical and numerical analyses, the geotechnical parameters of the units are determined. Results of the laboratory tests on the specimens obtained from the boreholes drilled in this section of the T8 tunnel are presented in Table 1. In addition, the input data used in the design stage are given in Table 2, and the core photographs of the boreholes are given in Fig. 4. A frequency histogram graphically integrated with descriptive

| Borehole No | Sample No | Depth | | Unit Weight | UCS | Young Modulus |
|---|---|---|---|---|---|---|
| | | Start | Finish | $\gamma_n$ (kN/m$^3$) | $\sigma_c$ (MPa) | $E_i$ (GPa) |
| T8-SK3 | C1 | 22.50 | | 23.76 | 2.08 | 0.30 |
| T8-SK3 | C2 | 34.50 | | 23.46 | - | - |
| T8-SK3 | C3 | 41.35 | | 25.09 | 0.71 | 0.54 |
| T8-SK3A | C1 | 25.25 | 25.50 | 22.98 | 1.55 | 0.42 |
| T8-SK3A | C2 | 37.00 | 37.45 | 19.93 | - | - |
| T8-SK4 | C1 | 17.00 | 18.00 | 24.57 | 3.08 | 4.51 |

*Tab. 1 - Laboratory test results (Fugro Sial, 2009)*

| Overburden thickness | Uniaxial strength | Geological strength index | Material constant | Elasticity modulus | Unit weight | Cohesion | Internal friction angle | Deformation modulus |
|---|---|---|---|---|---|---|---|---|
| H (m) | UCS (MPa) | GSI | $m_i$ | $E_i$ (MPa) | γ (kN/m³) | c (kPa) | Ø (°) | $E_m$ (MPa) |
| 55 | 5 | 25 | 6 | 1400 | 23 | 52 | 19 | 80 |

*Tab. 2 - Inputs used in geotechnical analyses*

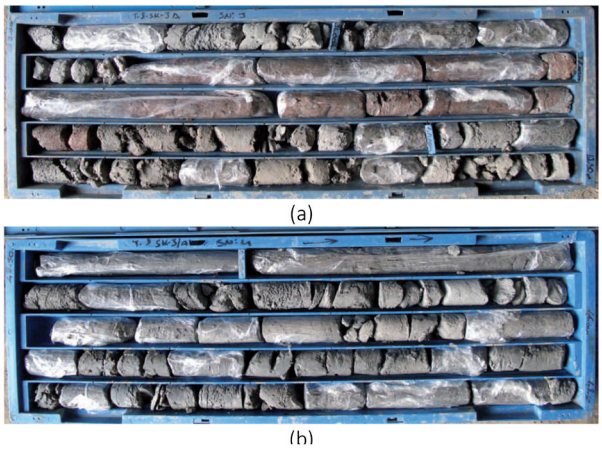


*Fig. 4 - T8-SK3A borehole photos between from 33.0 m to 42.50 m (a) and from 42.50 m to 48.50 m (Fugro Sial, 2009)*

statistics of the distribution of events with different magnitudes provides an immediate visual depiction of the descriptive metrics of the dataset and the relevant insights for our study (Fig. 4).

Considering the geological condition of the tunnel route, the average uniaxial compressive strength for the Abant Formation encountered in these sections was assigned as 2 MPa, taking into account the laboratory test results on the samples taken from the T8-SK3, T8-SK3a, and T8-SK4 boreholes, and the material constant was considered as $m_i$=4 for claystone since it very weak rock. The modulus of elasticity value was determined as 1.4 GPa. Geological Strength Index (GSI) value is determined as 25 according to the procedure suggested by Hoek & Marinos (2000). These parameters are used in the RocLab (Roclab, 2011) program, and the parameters of the rock mass are calculated for this section (Fig. 5).

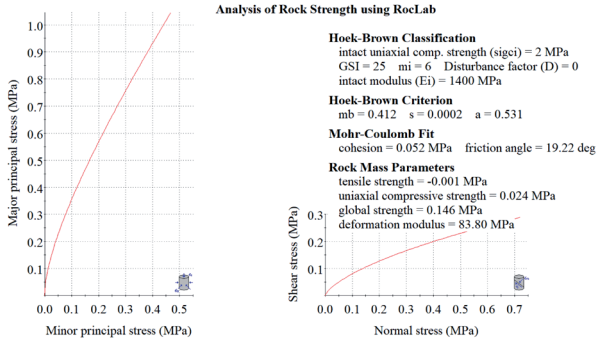


*Fig. 5 - Failure envelope for 55 m overburden thickness*

The rock mass parameters are calculated considering 55 m of overburden thickness, and the results are summarized in Table 3.

| Overburden thickness | Uniaxial strength | Geological strength index | Material constant | Elasticity modulus | Unit weight | Cohesion | Internal friction angle | Deformation modulus |
|---|---|---|---|---|---|---|---|---|
| H (m) | UCS (Mpa) | GSI | $m_i$ | $E_i$ (MPa) | γ (kN/m³) | c (kPa) | Ø (°) | $E_m$ (MPa) |
| 55 | 5 | 25 | 6 | 1400 | 23 | 52 | 19 | 80 |

*Tab. 3 - Geotechnical parameters of the tunnel for 55 m overburden thickness*

## *Determination of rock mass class*

The rock mass classes are examined with the RMR Classification System and NGI (Q) rock mass classification systems to determine the rock mass classes and determine the initial support systems for the tunnel.

## *RMR classification system*

The RMR Classification System was developed by Bieniawski (1973, 1976, 1989). The system has undergone several changes in the 15-year period until 1989, based on observations and new data. From 1973 to 1989, the system took its final shape within the framework of the data and experience gained from a total of 351 different applications related to tunnels, large underground openings, and mining operations (Bieniawski, 1989). The rock mass classification ratings (RMR) of the sections to be encountered in the tunnel opening were calculated according to Bieniawski (1989) (Table 4).

| A | Parameter | Value/Definition | Rating |
|---|---|---|---|
| 1 | Uniaxial compressive strength (MPa) | 2 | 1 |
| 2 | Rock quality designation (RQD %) | 10 | 4 |
| 3 | Spacing of discontinuites (mm) | 100 | 6 |
| 4 | Conditions of discontinuities | | |
| | Persistence | 10-20m | 1 |
| | Aperture | >5mm | 0 |
| | Roughness | Less Rough | 3 |
| | Fiiling | Soft infilling>5 mm | 0 |
| | Weathering | Highly weathered | 1 |
| 5 | Ground water | Dripping | 4 |
| | Basic RMR | | 20 |
| B | Discontinuity orientation | Fair | -5 |
| | Final RMR | Very poor rock mass | 15 |

*Tab. 4 - RMR classification input parameters*

According to the RMR rock classification system, this section of the tunnel is determined as very poor rock mass. For very poor rock mass, the support system proposed by Bieniawski (1989) is suggested by gradual excavation, systematic bolting, 15-20 cm thick shotcrete, 0.75 m spacing light or heavy steel rib.

## *Q Classification System*

The rock mass classification are performed by the Q or NGI

(Norvegian Geotechnical Institute) system (Barton *et alii*, 1974, 1981; Grimstad & Barton, 1993; Barton, 1993). Rock tunneling quality Q is calculated from the following expression as a function of 6 independent parameters. The Q value calculated according to the Q rock mass classification system is given in Table 5. The Q value is calculated with the help of Eq.1

$$Q = \frac{RQD}{Jn} x \frac{Jr}{Ja} x \frac{Jw}{SRF} \quad (1)$$

| No | Parameter | | Value/Definition | Rating |
|---|---|---|---|---|
| 1 | RQD | : Rock quality designation | A. Very poor | 10 |
| 2 | Jn | : Joint set number | F. Three joint sets | 9 |
| 3 | Jr | : Joint roughness number | H. Unaltered joint walls, surface staining only | 1 |
| 4 | Ja | : Joint alteration number | H. Medium or low over-consolidation, softening, clay mineral fillings (continuous but <5 mm thickness). | 8 |
| 5 | Jw | : Joint water reduction number | B. Medium inflow | 0,66 |
| 6 | SRF | : Stress reduction factor | A. Multiple occurrences of weak zones within a short section containing clay or chemically disintegrated, very loose surrounding rock (any depth), | 10 |

*Tab. 5 - Parameters of the Q classification system*

Accordingly, the Q value is calculated as 0.009, and the rock mass along the tunnel is classified as the exceptionally poor category (Fig. 6).

Consequently, according to both the RMR system and the Q rock classification system, the tunnel is in very weak rock mass conditions.

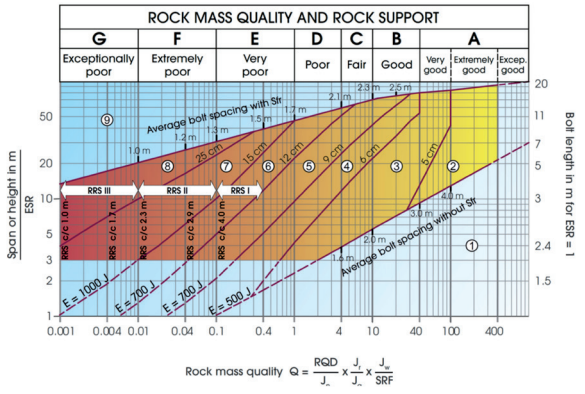


*Fig. 6 - Q rock mass classification system (NGI, 2015)*

## PROBLEMS ENCOUNTERED ALONG THE T8 TUNNEL

Between km: 142+000 - 142+480 in the T8 tunnel, the tunnel zone passes entirely in the brecciated fault zone (Fig. 7). In addition, due to the low overburden thickness in this section of the tunnel and the landslides, no arching is formed around the tunnel. Depending on the long-term swelling and squeezing properties of the clayey units,

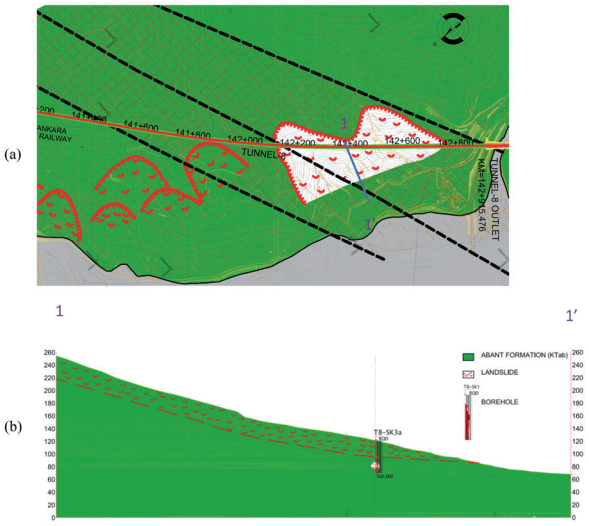


*Fig. 7 - (a) Geological map of the close vicinity of the studied section, and (b) Geological cross-section for the numerical analysis (km:142+380) (Section 1-1' on Fig. 7a)*

the loads on the supports have increased in this section and failures have occurred. During the tunnel excavation, serious deformations were observed in the tunnel due to these adverse conditions.

### *Convergence and optical measurements in the tunnel*

Deformation measurements were taken during the tunnel excavation. Results of the measurements taken at km:142+206.95 are given in Fig. 8.

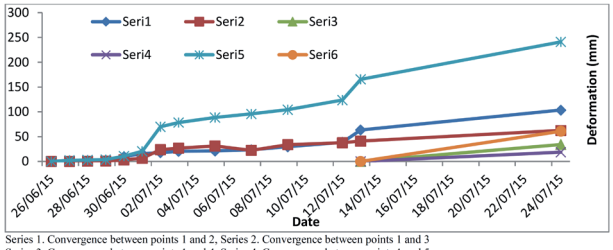


*Fig. 8 - Convergence measurement at Km:142+206.95*

When the deformation measurements are inspected, it is seen that it exceeds 25 cm in places. In addition, the measurements taken from the tunnel section revealed that the tunnel penetrated the section in most places (Fig.9).

The units of the Abant formation encountered during the tunnel excavation are given in Fig. 4. When the geological cross-section at km: 142+139.03 is examined, the ground is gray, black in color, weak-very weak strength claystone, and siltstone and it is classified as a compacted soil (C3) according to the tunnel rock class NATM class (ONORM B 2003, KGM

2013) (Fig. 10). In Fig.11, it is seen the failed bolts, and the longitudinal and transverse cracks on the shotcrete related to excessive deformation.

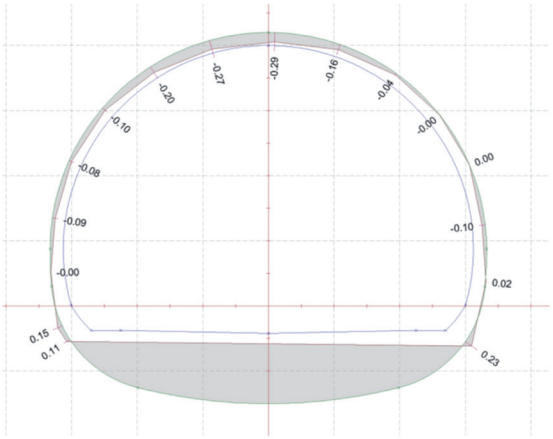


*Fig. 9 - Tunnel deformation section at km: 142+088*

*Fig. 10 - Tunnel face at km:142+139.03*

*Fig. 11 - Cracks in shotcrete and failures in bolts*

## EVALUATION OF TUNNEL SQUEEZING CONDITIONS AND TUNNEL BEHAVIOR

To evaluate the properties of the ground in the tunnel, it is important to examine both the ground reaction curve (GRC) and squeezing condition in the tunnel. For this purpose, Hoek and Marinos (2000), Jethwa *et alii* (1984), and Sakurai (1983) approaches are used (Table 6). They proposed equations depending on the compressive strength of the rock mass, the overburden thickness, and the in-situ pressure of the factors affecting the squeezing. Sakurai (1983) determined the strain value with Eq. (2) and showed it graphically according to the compressive strength of the rock mass. Jethwa *et alii* (1984), on the other hand, defined squeezing according to the $N_c$ value (Eq. 3), which is determined by the ratio of the compressive strength of the rock mass to the in-situ pressure. Hoek & Marinos (2000),

| Researchers | Equations |
|---|---|
| Sakurai (1983) | $\varepsilon_{pc}=1.073\sigma_{cm}^{-0.318}$ (2) |
| Jethwa et al. (1984) | $Nc=\frac{\sigma cm}{Po}=\frac{\sigma cm}{\gamma * h}$ (3) |
| Hoek and Marinos (2000) | $\varepsilon=0.2*(\sigma_{cm}/p_0)^{-2}$ (4) |

*Tab. 6 - Squeezing equations suggested by different researchers*

while defining compression, classified the strength of the rock mass according to the strain value determined by the ground pressure (Eq. 4).

According to Sakurai (1983), the $\varepsilon_{pc}$ value is found to be 2.0 and it is stated that special support systems would be needed in the tunnels. On the other hand, Jethwa *et alii* (1984) determined that the $N_c$ value was 0.11 and it is stated that high squeezing is expected. Hoek & Marinos (2000) found the $\varepsilon$ value to be 16 and stated that serious stability problems would be encountered in the tunnel. Closed-form solutions (Hoek & Brown, 1980; Hoek 2007 and 2012) equations are used to determine the tunnel ground reaction curve. With the help of these equations, the radius of the plastic zone around the tunnel, elastic and plastic deformations, and strain values are determined. The in-situ pressure at 55 m overburden thickness is calculated as $P_0$=0.022*55=1.1 MPa. If the compressive strength of the rock mass is σcm, it is 0.14 MPa, and the $\sigma_{cm}/P_0$ ratio is 0.13. The displacement at the tunnel face is 28 cm and the plastic displacement around the tunnel is 2.07 m (Table 7).

| Rock mass strength $\sigma_{cm}$ | In situ stress $P_0$ | $\sigma_{cm}/P_0$ | Plastic zone radius $r_p$ (m) | Strain $\varepsilon$ (%) | Total deformation $u_i$ (m) | Tunnel face deformation $u_{if}$ (m) | Critical support pressure $P_{cr}$ (MPa) |
|---|---|---|---|---|---|---|---|
| 0.14 | 1.26 | 0.14 | 38 | 11 | 0.41 | 0.28 | 0.69 |

*Tab. 7 - Analytical solution results (Hoek & Brown, 1980; Hoek 2007 and 2012)*

The variation of the soil reaction curve (GRC) and the radius of the plastic zone is given in Fig. 12. Here, it is seen

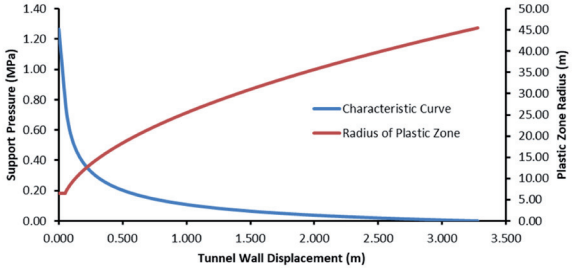


*Fig. 12 - Longitudinal displacement profile for h=55 m*

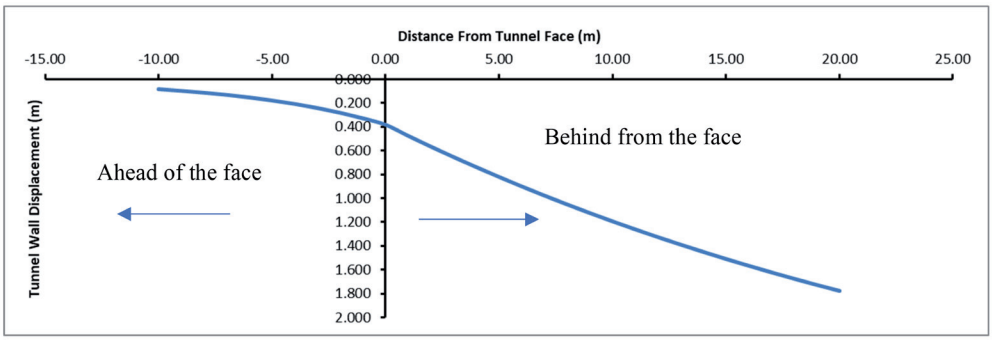


*Fig. 13 - Longitudinal displacement profile for h=55 m*

that the radius of the plastic zone and the soil reaction curve develop very rapidly.

In addition, Vlachopoulos & Diederichs (2009) approach is used to draw a Longitudinal Displacement Profile along the tunnel (Fig. 13).

In the unsupported condition, 38 cm deformation occurs in the tunnel face, while this value increases to 57 cm 1 m behind the face. 20 m behind the face, the deformations go up to 1.78 m. As can be seen, serious deformations occur both in the tunnel face and in the tunnel behind the tunnel under 55 m overburden thickness.

## ASSESSMENT OF TUNNEL SUPPORT SYSTEMS

This section of the tunnel is determined as C3 rock class which is squeezing conditions (KGM, 2013 and ONORM B2203, 2001) according to the NATM rock classification system. In this section, the C3 support system was chosen as the tunnel support system, and the support system properties are given in Fig.14 and Tables 8 and 9.

The support system pressure ($P_{ssmax}$) and stiffness ($K_{ss}$) determined for INP 200 type steel rib are given in Eqs. 2 and 3.

$$Pssmax = \frac{\mathrm{As} * \sigma ys}{sl * lro} \quad (2)$$

$$Kssmax = \frac{\mathrm{Es} * As}{sl * lro^2} \quad (3)$$

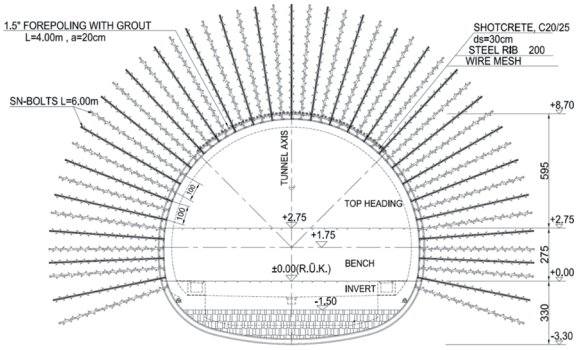


*Fig. 14 - C3 support system details*

The strength properties of C20/25 type shotcrete are given in Table 10. The support system pressure Pscmax and stiffness $K_{sc}$ of the shotcrete are presented in Eqs. 4 and 5, respectively.

$$Pscmax = \frac{\sigma cc}{s} * \left[1 - \frac{(ro - tc)^2}{ro^2}\right] \quad (4)$$

| Round length | Shotcrete | Steel rib | Wire mesh | Bolts | Forepoling |
|---|---|---|---|---|---|
| 1.0 m Top heading, 2.0 m bench, 4.0 m Invert | C20/25, 30 cm | I 200 | Q221/221 2 layer | Fully grouted bolt, SN type, 6 m (1.0x1.0 m pattern) | 1.5" grouted, L=6 m |

*Tab. 8 - Summary of the C3 support system*

| $A_s$ ($m^2$) | $s_l$ (m) | $E_s$ (MPa) | $\sigma_{ys}$ (MPa) | Pssmax (MPa) | Kss (MPa/m) |
|---|---|---|---|---|---|
| Cross sectional area | Spacing along the tunnel axis | Young Modulus of the steel rib | Yield strength of the steel | Support pressure | Stiffness |
| 0.00334 | 1 | 207000 | 365 | 0.187 | 16.364 |

*Tab. 9 - I200 type steel rib properties, $P_{ssmax}$ and $K_{ssmax}$*

| $t_c$ (m) | $\nu_c$ | $E_c$ (MPa) | $\sigma_{cc}$ (MPa) | Pscmax (MPa) | Ksc (MPa/m) |
|---|---|---|---|---|---|
| Thickness of the shotcrete | Poisson ratio | Young modulus of the shotcrete | Uniaxial compressive strength of the shotcrete | Support pressure | Stiffness |
| 0.3 | 0.2 | 28000 | 20 | 0.90 | 212.1 |

*Tab. 10 - C20/25 type shotcrete properties, $P_{scmax}$ and $K_{scmax}$*

| $d_b$ (m) | l (m) | $E_s$ (MPa) | $s_c$ (m) | $s_l$ (m) | $T_{bf}$ (MN) | Psbmax (MPa) | Ksb (MPa/m) |
|---|---|---|---|---|---|---|---|
| Bolt diameter | Length | Young Modulus | Circumferential bolt spacing | Longitudinal bolt spacing | Ultimate bolt load | Support pressure | Stiffness |
| 0.026 | 6 | 207000 | 1 | 11 | 0.125 | 0.125 | 18.137 |

*Tab. 11 - Bolt properties, $P_{sbmax}$ and $K_{sbmax}$*

$$Ksc = \left( Ec * \frac{ro^2 - (r0 - tc)^2}{2 * (1 - \vartheta^2) * (r0 - tc) * ro^2} \right) \quad (5)$$

The properties of the bolts used in the tunnel are given in Table 11. The support pressure $P_{sbmax}$ and stiffness $K_{sb}$ values of the bolts are shown in Eqs. 6-7.

$$Psbmax = \frac{Tbf}{sl*sc} \quad (6)$$

$$Ksb = Es * \pi * \frac{db^2}{4lslsc} \quad (7)$$

The total support pressure system is calculated as $Pt=P_{sbmax}+P_{scmax}+P_{ssmax}$=1.21 MPa. The critical pressure ($P_{cr}$) for the tunnel support system is determined as 0.81 MPa. The ground reaction curve and support reaction curve are given in Fig. 15.

Since the pressure ($P_i$) of the tunnel support systems is higher than the critical pressure ($P_{cr}$), no plastic deformation is expected in the tunnel. The ratio support pressure to critical pressure is nearly 1.5.

Also, during the tunnel excavation encountered problems, the standard bolts were changed to the IBO (self boring bolt) bolts to achieved much better groutin around the tunnel. Additionally, for roof stability, 1.5" diameter forepolings were replaced with a 3.5" diameter umbrella system. After application of these revisions, the tunnel face and roof stability is ensured.

## 3D NUMERICAL ANALYSES

*Flac 3D* (Itasca, 2002) program is used to understand the relationship between the problems in the tunnel and the landslide. For this purpose, the model ranges from Km: 142+300 - 142+380. This part of the tunnel is the closest to the landslide, and the failure

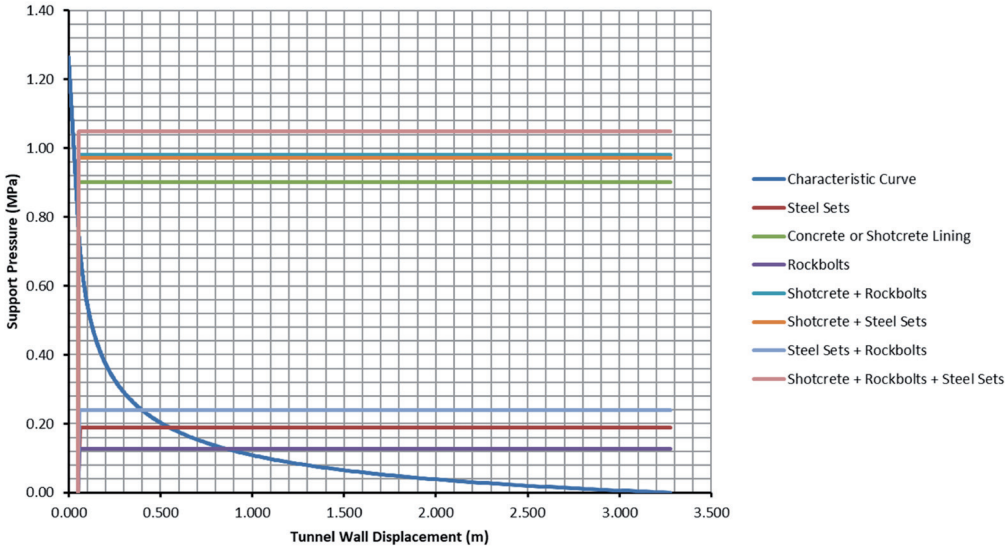


*Fig. 15 - Support reaction curve*

surface of the landslide is approximately 15 m above the tunnel. The model created with the *Flac 3D* program is given in Fig 16. The upper part of the model represents the landslide and the lower part is the in place the units of the Abant formation. In the analysis, excavation stages are given in the form of model top heading,

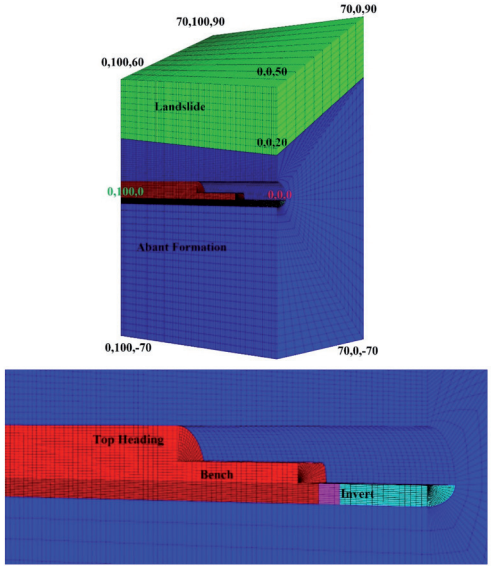


*Fig. 16 - Flac3d numerical model*

bench and invert. The excavation stages are shown in Table 12. Analyses are performed in 16 stages. In the analyses, it is assumed that the excavation and support of the first 40 m in the top heading, the first 20 m in the bench, and the first 16 m in the invert section. Afterwards, excavation is carried out in stages in the top heading, bench, and invert sections. Mohr-Coulomb failure criterion is used in the model, and the gravity method is chosen in the analysis. For this, the upper side of the model is defined as free in the x, y and z directions. To minimize the effect of boundary conditions in the model, the distance between boundary is 5D. The model is 70 m in the X direction, 120 m in the Z direction and 100 m in the Y direction, and the tunnel coordinates are given in Fig.17.

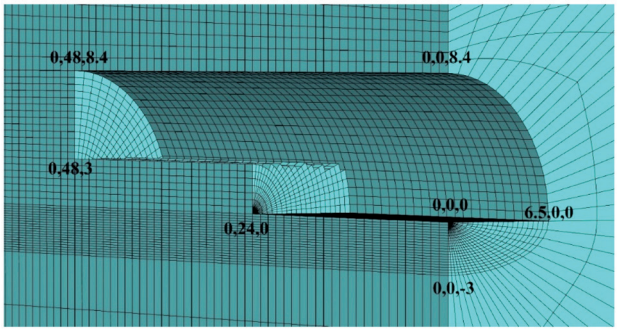


*Fig. 17 - Tunnel coordinates*

## *Deformations in the tunnel*

The deformations that occurred during the excavation in the tunnel are plotted in horizontal and vertical directions. For this purpose, points were identified on the tunnel roof and at the bottom of the tunnel. The displacements depending on the excavation at the determined points are shown graphically. The deformations occurring in the vertical direction (Z direction) at points 2 and 9 on the tunnel roof are given in Fig.18. Deformation history points are 2 m, 4 m, 6 m, 8 m, 12 m, 16 m, 24 m and 26 m in Y direction at tunnel roof. The coordinates of the determined history points are presented in Table 13. As can be seen from here, deformations are observed at the maximum level of 4.3 cm at the tunnel roof at the beginning of the tunnel (0, 0, 0) and up to 26 m. While the deformations in the first 12 m of the tunnel are between 3.5 cm and 4.3 cm, they are at the level of 2.98 cm at 16

| Stage | Step | Excavation Situation | Stage | Step | Excavation Situation |
|---|---|---|---|---|---|
| 1 | 1500 | Unbalanced forces | 9 | 13500 | Excavation between 43-44 m in TH |
| 2 | 3000 | Excavation between 0-40 m full face excavation and 0-20 m top heading excavation, 0-16 m invert excavation, installation supports and installation inner lining concrete, and reset displacements | 10 | 15000 | Excavation between 22-23 m in Bench |
| 3 | 4500 | Excavation between 40-41 m in TH | 11 | 16500 | Excavation between 44-45 m in TH |
| 4 | 6000 | Excavation between 41-42 m in TH | 12 | 18000 | Excavation between 45-46 m in TH |
| 5 | 7500 | Excavation between 20-21 m in Bench | 13 | 19500 | Excavation between 23-24 m in Bench |
| 6 | 9000 | Excavation between 21-22 m in Bench | 14 | 21000 | Excavation between 20-22 m in invert |
| 7 | 10500 | Excavation between 16-20 m in invert | 15 | 22500 | Excavation between 46-47 m in TH |
| 8 | 1200 | Excavation between 42-43 m in TH | 16 | 24000 | Excavation between 47-48 m in TH |

*Tab. 12 - Modelling stages*

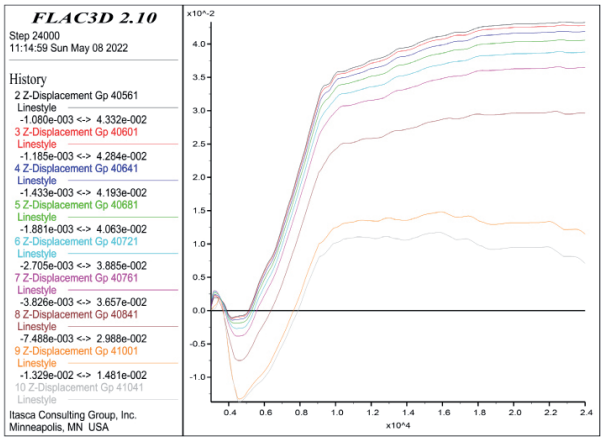


*Fig. 18 - Vertical displacements (z direction) in history points 2 to 9*

| HP | 2 | 3 | 4 | 5 | 6 | 7 | 8 | 9 | 10 |
|---|---|---|---|---|---|---|---|---|---|
| Co | 0,2,8.4 | 0,4,8.4 | 0,6,8.4 | 0,8,8.4 | 0,10,8.4 | 0,12,8.4 | 0,16,8.4 | 0,24,8.4 | 0,26,8.4 |

HP: History Points, Co: Coordinates (x, y, z)

*Tab. 13 - History points coordinates from 2 to 10*

m, 1.48 cm at 24 m and 0.75 cm at 26 m. In a sense, the effect of tunnel excavations remains constant after 2 diameters of the tunnel. Considering that the tunnel diameter is 13 m, the increase in tunnel deformations continues at 26 m behind the tunnel face, that is, at 12 m.

Vertical displacements between 28 and 52 m are presented in Fig. 19. In Table 14, the coordinates of the determined points are given. Deformation history points are 28 m, 30 m, 40 m, 42 m, 44 m, 46 m, 48 m, 50 m and 52 m in Y direction at tunnel ceiling. Tunnel excavation is carried out up to 48 m, and deformations

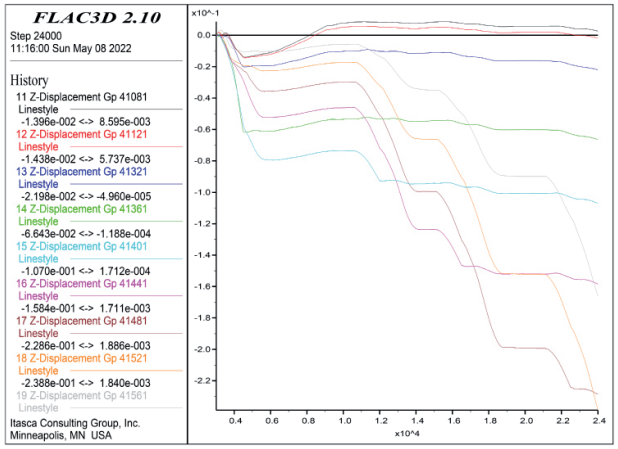


*Fig. 19 - Vertical displacements (z direction) in history points 11 to 19*

| HP | 11 | 12 | 13 | 14 | 15 | 16 | 17 | 18 | 19 |
|---|---|---|---|---|---|---|---|---|---|
| Co | 0,28,8.4 | 0,30,8.4 | 0,40,8.4 | 0,42,8.4 | 0,44,8.4 | 0,46,8.4 | 0,48,8.4 | 0,50,8.4 | 0,52,8.4 |

HP: History Points, Co: Coordinates (x,y,z)

*Tab. 14 - History points coordinates from 11 to 19*

are examined in the section where the tunnel is excavated at 50 and 52 m. The largest deformations occurred at 48 and 50 m and increased up to 23 cm. It is observed that the deformations increased immediately after the excavation. At 28 m, 30 m, 40 and 42 m, the deformations are at the maximum level of 6 cm. However, the rate of increase in deformations increased from 44 m to 15 cm, 22 cm, and 24 cm. This situation showed us that while no significant increase was observed 2 m behind the tunnel, the section where the tunnel is most affected occurred in the first 2 m section.

The deformations in the horizontal direction given in Fig. 20 for the first 20 m of the tunnel. The determined historical points are also given in Table 15. Deformation history points are 2 m, 4 m, 6 m, 8 m, 10 m, 12 m, 14 m, 16 m and 20 m in X direction at tunnel side wall. In this section, the top heading, bench and invert excavations of the tunnel have been completed. The horizontal deformations in this section remained at the mm level and arching has been achieved in the tunnel. In other words, after a distance of 2 diameters of the tunnel, 26 m behind the tunnel face, it is seen that the tunnel excavation does not have a serious effect on the stability.

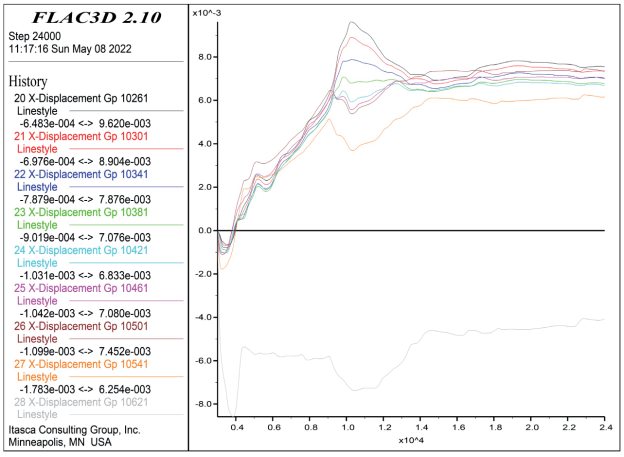


*Fig. 20 - Horizontal displacements (x direction) in hist points 20 to 28*

| HP | 20 | 21 | 22 | 23 | 24 | 25 | 26 | 27 | 28 |
|---|---|---|---|---|---|---|---|---|---|
| Co | 6.5,2,2.75 | 6.5,4,2.75 | 6.5,6, 2.75 | 6.5,8, 2.75 | 6.5,10, 2.75 | 6.5,12, 2.75 | 6.5,14, 2.75 | 6.5,16, 2.75 | 6.5,20, 2.75 |

HP: History Points, Co: Coordinates (x,y,z)

*Tab. 15 - History points coordinates from 20 to 28*

In Fig. 21, horizontal displacements between 24 m and 50 m in the tunnel are presented. The coordinates of these notes are given in Tables 16 and 17. Deformation history points are 24 m, 26 m, 28 m, 30 m, 40 m, 44 m, 46 m, 48 m and 50 m in X direction at tunnel side wall. Horizontal deformations in the upper half of the tunnel due to tunnel excavation are up to 20 cm. The horizontal deformations between the 24 m, 26 m, 28 m and 30 m of the

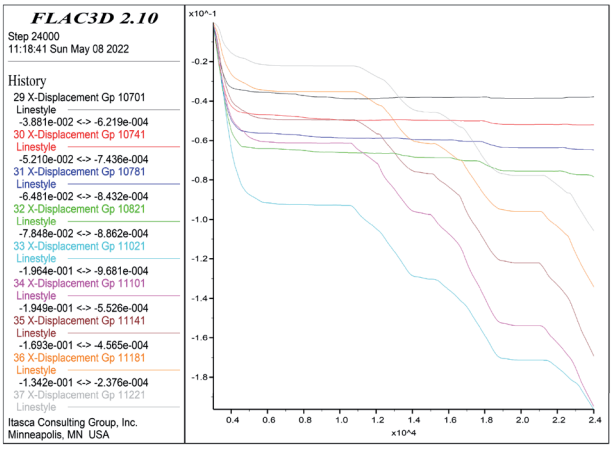


*Fig. 21 - Horizontal displacements (x direction) in history points 29 to 37*

| HP | 29 | 30 | 31 | 32 | 33 |
|---|---|---|---|---|---|
| Co | 6.5,24,2.75 | 6.5,26,2.75 | 6.5,28,2.75 | 6.5,30,2.75 | 6.5,40,2.75 |

*Tab. 16 - History points coordinates from 29 to 33*

| HP | 34 | 35 | 36 | 37 |
|---|---|---|---|---|
| Co | 6.5,44,2.75 | 6.5,46,2.75 | 6.5,48,2.75 | 6.5,50,2.75 |

*Tab. 17 - History points coordinates from 34 to 37*

tunnel remained at the level of 6.4 cm and remained constant. In other words, it is seen that the effect on horizontal displacements in the tunnels is not serious starting from 18 m behind the face excavation of the tunnel. From 40 m, the deformations increased up to 20 cm. It is seen that the deformations reach the maximum level 8 m behind the tunnel face.

Vertical displacements at the tunnel floor are given in Fig. 22. The coordinates of the determined points are presented in Table 18. Deformation history points are 4 m, 6 m, 8 m, 10 m,

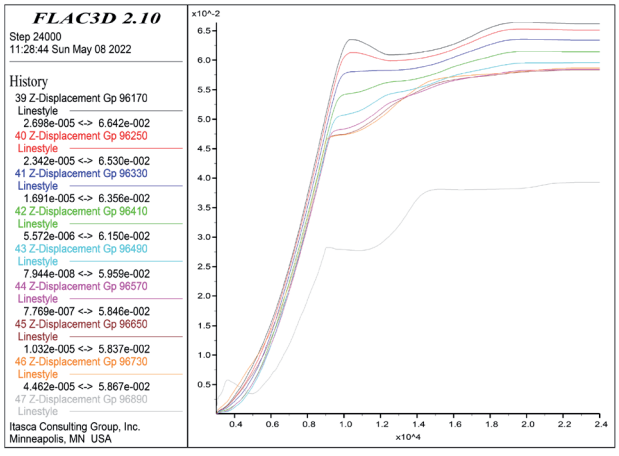


*Fig. 22 - Vertical displacements (Z direction) in history points 39 to 47*

| HP | 39 | 40 | 41 | 42 | 43 | 44 | 45 | 46 | 47 |
|---|---|---|---|---|---|---|---|---|---|
| Co | 0,4,-3 | 0,6,-3 | 0,8,-3 | 0,10,-3 | 0,12,-3 | 0,14,-3 | 0,16,-3 | 0,20,-3 | 0,24,-3 |

*Tab. 18 - History points coordinates from 39 to 47*

12 m, 14 m, 16 m, 20 m and 24 m in Z direction at tunnel invert. The vertical displacements at the bottom of the tunnel occur at a maximum level of 6.6 cm. These displacements continue after the completion of the invert excavations, that is, after 11500 steps.

The vertical displacements occurring in the bottom part of the tunnel are given in Fig 23. The coordinates of these points are presented in Table 19. Deformation history points are 4 m, 6 m, 8 m, 10 m, 12 m, 14 m, 16 m, 20 m and 24 m in Z direction at tunnel invert. Here, the largest displacement in the invert section occurs in the tunnel excavation face as 15.8 cm. 18 m behind the tunnel face, the deformations remained at the level of 3 cm and continued steadily. It is seen that the tunnel excavation face is fixed 18 m behind the effect of the base part.

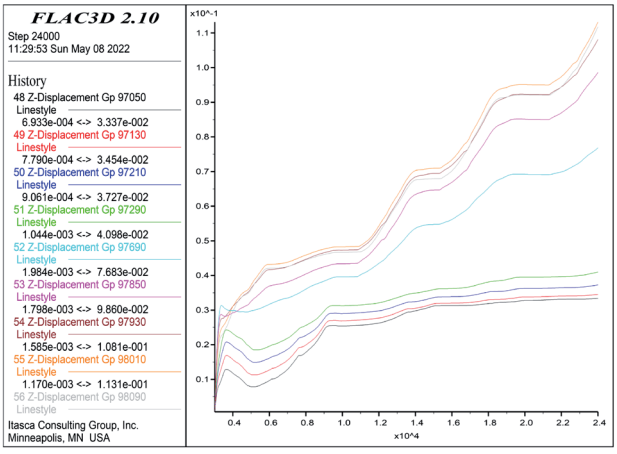


*Fig. 23 - Vertical displacements (Z direction) in history points 48 to 56*

| HP | 48 | 49 | 50 | 51 | 52 | 53 | 54 | 55 | 56 |
|---|---|---|---|---|---|---|---|---|---|
| Co | 0,4,-3 | 0,6,-3 | 0,8,-3 | 0,10,-3 | 0,12,-3 | 0,14,-3 | 0,16,-3 | 0,20,-3 | 0,24,-3 |

*Tab. 19 - History points coordinates from 48 to 56*

## *Deformations in the landslide zone*

To evaluate the relationship between the landslide on the tunnel and the tunnel excavation, points are determined in the landslide area. At these points, deformations are drawn due to tunnel excavation. Zhu *et alii* (2022) investigated the triggering mechanism of a tunneling induced - landslide employing 2D numerical analysis while Sun *et alii* (2022) studied adverse landslide effect on tunnel by combining model testing and numerical simulation.

## *Examination of the base section of the landslide*

The displacements occurring between 45 m and 37 m in

the landslide section are given in Fig. 24 and the determined coordinates are given in Table 20. The largest displacements occurred at the level of 1.7 cm.

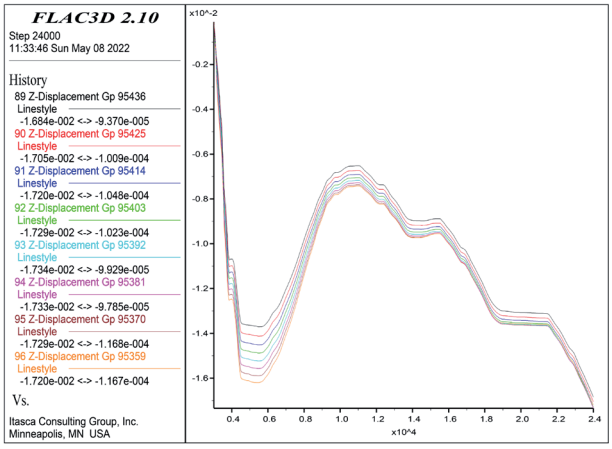


*Fig. 24 - Vertical displacements (Z direction) in history points 80 to 88 in the landslide section*

| HP | 89 | 90 | 91 | 92 | 93 | 94 | 95 | 96 |
|---|---|---|---|---|---|---|---|---|
| Co | 0,45,54.5 | 0,44,54.4 | 0,43,54.3 | 0,42,54.2 | 0,41,54.1 | 0,40,54.00 | 0,39,53.9 | 0,38,53.8 |

*Tab. 20 - History points coordinates from 89 to 96*

### *Displacements in the crown of the landslide*

The displacement graph that occurred at the crown of the landslide is given in Fig. 25, and the coordinates of the determined history points are given in Table 21. The displacements that occur at a maximum level of 2.6 cm.

As can be seen, the deformations that occur in the landslide zone with the tunnel excavation are 2.6 cm in the roof and 1.7 cm in the toe part.

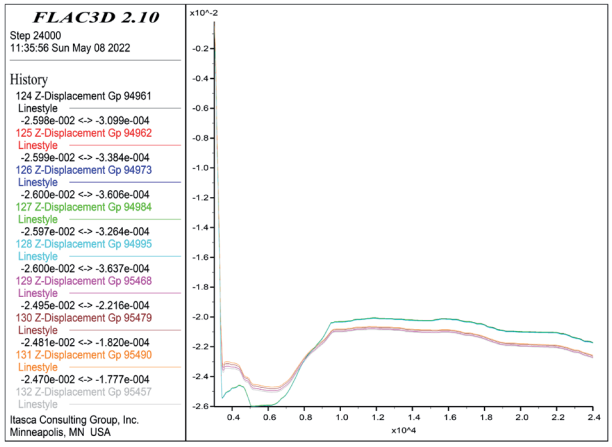


*Fig. 25 - Vertical displacements (Z direction) in history points 124 to 132 in the landslide section*

| HP | 124 | 125 | 126 | 127 | 128 | 129 | 130 | 131 |
|---|---|---|---|---|---|---|---|---|
| Co | 70,0,90 | 70,1,90 | 70,3,90 | 70,4,90 | 70,47,90 | 70,48,90, | 70,49,90 | 70,49,90 |

*Tab. 21 - History points coordinates from 124 to 131*

### *Comparison of field measurements and numerical analysis results of landslide deformation*

According to the numerical analysis, the maximum vertical displacement occurred at the level of 24 cm. Similarly, in horizontal deformations, it is at the maximum level of 18 cm. In the measurements performed in the field, it is seen that the deformations in the tunnel occur between 22 cm and 27 cm. As can be seen, it is seen that there is a consistency in the field measurements with the numerical analyses.

## CONCLUSIONS

In the study, the possible causes of the excessive deformations during a high-speed railwal tunnel construction in poor geotechnical conditions and under a landslide zone are presented. It is evident that existence of landslides on the tunnel route adversely affects the deformations. Although the failure surface does not cut the tunnel in this case, there is no a direct interaction between landslide and tunnel. For this reason, the details of the indirect interaction are investigated. For the purpose of the study, 3D numerical analyzes are performed. The results obtained from the analyses and the results of the in-situ measurements showed consistency. Closing the ring during tunnel excavation is very important for tunnel stability. One of the most important conclusions obtained from the study is that the distance between the tunnel and the failure surface of the landslide should not be less than 10 m in tunnels to be excavated under landslides. Because both in the field measurements and in the numerical analysis, it is observed that the indirect landslide effect of the tunnel excavation exists but it is limited. The T8 tunnel was constructed succesfully, and it is open to traffic and no problems have been encountered.

The excessive deformations occurred in the tunnel generally terminated behind the 2D distance. Closing the ring in 2D distance on weak ground affect positively the stability of the tunnel.

The support pressure ($P_i$) is 1.21 MPa and the critical pressure ($P_{cr}$) is 0.81 MPa. The ratio between support pressure to critical pressure is 1.5. When selecting the support systems for non-deformational section, the support pressure should be 1.5 times critical support pressure. Also, during the tunnel excavation encountered problems, IBO bolts and 3.5” diameter umbrella system were used to ensure for tunnel face and roof stability.

The source of the deformations and failures in the tunnel is due to the high horizontal pressures, and this is the indirect adverse effect of the landslide material on the tunnel. However, despite the deformations in the tunnel, the stability of the tunnel was ensured as a result of reprofiling and additional supporting works. The

design of the tunnel support system should be rigid to minimize the deformations under swelling conditons and landslide zone.

As stated by Tian (2021), "the reinforcement measures for controlling slope deformation may be ineffective for preventing slope sliding, owing to the lack of a clear understanding regarding the slope failure and tunnel deformation modes". For this reason, the study peresented herein can be accepted as an effort for understanding the possible indirect adverse effect on tunnel excavationsç Consequently, the presented study provides a scientific basis for future tunnel constructions under landslides.

## ACKNOWLEDGMENTS

The authors would like to thank to General Directorate of State Railways of Turkey for the data support.

## REFERENCES

Ayoublou F.F., Taromi M. & Eftekharic A. (2019) - *Tunnel portal instability in landslide ares ad remedial solution, a case study*. Acta Polytechnica, **59**(5): 435-447, Doi:10.14311/ap.2019.59.0435.

Aygar E. B. (2000) - *A critical approach to the new Austrian tunneling method in Bolu tunnels* M.Sc Dissertation. Hacettepe University, Ankara, Turkey.

Aygar E.B. (2007) - *Investigation of the Bolu Tunnel stability by means of static and dyanamic analyses* Ph.D Dissertation. Hacettepe University, Ankara, Turkey.

Aygar E.B. (2020) - *Evaluation of new austrian tunnelling method applied to Bolu tunnel's weak rocks*. Journal of Rock Mechanics and Geotechnical Engineering, **12**:541-556, https://doi.org/10.1016/j.jrmge.2019.12.011.

Aygar E.B. & Gokçeoglu C. (2019) - *Ankara-Istanbul high-speed railway projects, T26 tunnel design and evaluation of support systems.* Proceedings of the 26th International Mining Congress and Exhibition of Turkey, IMCET 2019, Antalya, Turkey, April 16-19.

Aygar E. B. & Gokceoglu C. (2021) - *Effects of portal failure on tunnel support systems in a highway tunnel.* Geotech. Geol. Eng, **39**: 5707-5726, https://doi.org/10.1007/s10706-021-01859-z.

Bandini A., Berry P. & Boldini D. (2015) - *Tunneling-induced landslides: the val di gambro tunnel case study.* Engineering Geology **196**(9): 71-87.

Barla G., Debernardi D. & Perino A. (2015) - *Lessons learned from deep-seated landslides activated by tunnel excavation.* Geomechanics and Tunnelling, **8**(5): 394-401.

Barton N. (1993) - *Application of q-system and index tests to estimate shear strength and deformability of rock masses.* In Workshop on Norwegian Method of Tunnelling: 66-84. New Delhi, India.

Bieniawski Z.T. (1973) - *Engineering classification of jointed rock masses.* Trans S. Afr. Inst. Civ. Engrs **15**: 335-344.

Bieniawski Z.T. (1976) - *Rock mass classification in rock engineering.* In Exploration for rock engineering, Proc. of the symp., (ed. Z.T. Bieniawski) **1**: 97-106. Cape Town: Balkema.

Bieniawski Z.T. (1989) - *Engineering Rock Mass Classifications.* New York: Wiley.

Barton N.R., Lien R. & Lunde J. (1974) - *Engineering classification of rock masses for the design of tunnel support.* Rock Mech. **6**(4): 189-239.

Barton N.R., Løset F., Lien J. & Lunde R. J. (1981) - *Application of the q-system in design decisions.* In Subsurface space, (ed. M. Bergman), **2**: 553-561. New York: Pergamon.

Causse L., Cojean T. & Fleurisson J. (2015) - *Interaction between tunnel and unstable slope - influence of time-dependent behavior of a tunnel excavation in a deep-seated gravitational slope deformation.* Tunnelling and Underground Space Technology, **50**: 270-281.

Fugro Sial Geosciences Consulting & Engineering Ltd. (2009) - *T8 tunnel geological-geotechnical investigation report & tunnel project report.*

Gattinoni P., Consonni M. V., Francani V., Leonelli G. & Lorenzo C. (2019) - *Tunnelling in landslide areas connected to deep seated gravitational deformations: An example in Central Alps (northern Italy)*. Tunnelling and Underground Space Technology, **93**: 103100.

Gokceoglu C. & Karahan S. (2023) - *Seismic Performance of Transportation Tunnels in the Region Affected by the 6 February 2023 Türkiye Earthquake Sequence: A General Assessment*. 57th U.S. Rock Mechanics/Geomechanics Symposium, Atlanta, USA, ARMA 23-0960.

Gokceoglu C., Nefeslioglu H.A. & Tanyildiz N. (2014) - *A Decision Support System Suggestion for the Optimum Railway Route Selection.* 12th International IAEG Congress, Torino, Italy, **5**: 331-334, 10.1007/978-3-319-09048-1_63.

Gokceoglu C., Aygar E.B., Nefesliogiu H.A., Karahan S. & Gullu S. (2022) - *A Geotechnical Perspective on a Complex Geological Environment in a High-Speed Railway Tunnel Excavation (A Case Study from Türkiye).* Infrastructures, **7**: 155. https://doi.org/10.3390/infrastructures7110155.

Grimstad E. & Barton, N. (1993) - *Updating the q-system for ntm.* In: Kompen, Opsahl, Berg (eds.), Proceedings of the International Symposium on Sprayed Concrete – Modern Use of West Mix Sprayed Concrete for Underground Support. Fagernes, Osls.

Hoek E. (2007) - *Practical rock engineering.* **341**, https://www.rocscience.com/assets/resources/learning/ hoek/Practical-Rock-Engineering-Full-Text.pdf.

Hoek E. (2012) - *Rock support interaction analysis for tunnels in weak rcok masses*. https://www.rocscience.com/documents/pdfs/rocnews/winter2012/Rock-Support-Interaction-Analysis-for-tunnels-hoek.pdf.

Hoek E. & Brown E.T. (1980) - *Underground excavations in rock*. London: Instn Min. Metall.

Hoek E. & Brown E.T. (1997) - *Practical estimates or rock mass strength*. Int. J. Rock Mech. Min.g Sci. & Geomech. Abstr., **34**(8): 1165-1186.

Hoek E. & Marinos P. (2000) - *Predicting tunnel squeezing.* Tunnels and Tunnelling International, Part 1 – November 2000, Part 2 – December 2000.

Huang R. & Xiao H. (2010) - *Deformation mechanism of a shallow double-arch tunnel in a sloping rock mass*. Bulletin of Engineering Geology and the Environment, **69**(1): 89-97.

Hungr O. & McDougall S. (2009) - *Two numerical models for landslide dynamic analysis*. Computers and Geosciences, **35**(5): 978-992.

Itasca (2002) - *Flac 3D*, User Manual Getting Started.

Jethwa J. L. (1981) - *Evaluation of rock pressures in tunnels through squeezing ground in lower Himalayas*. Ph.D Dissertation, Department of Civil Engineering, University of Roorkee, India, 272.

KGM (General Directorate of Highways) (2013) - *Technical specifications of general directorate of highways*. Ankara, Turkey.

Kim N., Park D., Jung,H. & Kim M. (2020) - *Deformation characteristics of tunnel bottom after construction under geological conditions of long-term deformation.* Geomechanics and Engineering, **21**(2): 171-178. doi: https://doi.org/10.12989/gae.2020.21.2.171.

Komu M. P., Guney U., Kilickaya T. E. & Gokceoglu C. (2020) - *Using 3D numerical analysis for the assessment of tunnel–landslide relationship: Bahce–Nurdag tunnel (south of Turkey).* Geotechnical and Geological Engineering, **38**: 1237-1254.

Lunardi P., Cassani G. & Gatti, M. (2017) - *Planning of tunnels in landslides situation: the experience in the Italian Apennines*. Proceedings of the World Tunnel Congress 2017 – Surface challenges – Underground solutions, Bergen, Norway.

Manasa H. & Maji V.B. (2023) - *A Numerical Study on the Effect of Different Tunnel Shapes in Squeezing Rocks*. Indian Geotech. J., https://doi.org/10.1007/s40098-023-00782-9

Minglei S., Hongwei L., Yongquan Z., Xinqiang G., Huan L. & Zhengguo Z. (2022) - *Deformation and Failure Mode Analysis of the Tunnel Structure Based on the Tunnel-Related Landslides Cases*. Front. Earth Sci., **10**, https://doi.org/10.3389/feart.2022.906884.

Muller L. (1978) - *Removing misconceptions on the new Austrian tunnelling method*. Tunnels & Tunnelling International, **10**(8): 29-32.

NGI (2015) - *Using the Q system, rock mass classification and support design*. Handbook, Oslo, May 2015, https://www.ngi.no/eng/Services/Technical-expertise/Engineering-geology-and-rock-mechanics/Q-system.

Onorm B. 2203 (2001) - *(O¨sterreichisches Normungsinstitut), (1994).* Untertagebauarbeiten-Werkvertrag-snorm. Wien.

Özer C., Çevikbaş, A. & Eyüpoğlu M. (2013) - *Çamyurdu (Mudurnu-Bolu), Kirpiyen (Geyve-Sakarya) ryhsat sahaları maden jeolojisi ve prospeksiyon çalışmaları*. MTA Ekonomi Bültenleri, 2013_16.

Rabcewicz L. 1964a - *The New Austrian Tunnelling Method, Part One*. Water Power: 453-7.

Rabcewicz L. 1964b - *The New Austrian Tunnelling Method, Part Two*. Water Power 1964b: 511-5.

Rabcewicz L. 1965 - *The New Austrian Tunnelling Method, Part Three*. Water Power 1965: 19-24.

Rabcewicz L. & Golser J. 1973 - *Principles of dimensioning the supporting system for the "New Austrian Tunnelling Method*. Water Power, Marc,:88-93.

Roclab version 1.032 (2011) - www.rocscience.com.

Ruggeri P., Fruzzetti V.M.E., Vita A., Aternesi A., Scarpelli G. & Segato D. (2016) - *Deep-seated landslide triggered by tunnel excavation, Landslides and Engineered Slopes. Experience, Theory and Practice*. Proceedings of the 12th International Symposium on Landslides Napoli, Italy.

Sakurai S. (1983) - *Displacement measurements associated with the design of underground openings*. Proc. Int. Symp. Field Measurements in Geomechanics, Zurich **2**: 1163-1178.

Shrestha P.K., Panthi K.K. (2014) - *Groundwater Effect on Faulted Rock Mass: An evaluation of Modi Khola pressure tunnel in the Nepal Himalaya*. Rock Mech. Rock. Eng., **47**: 1021-1035. doi.org/10.1007/s00603-013-0467-7.

Sun Z., Yang X., Lu S., Chen Y. & Li P. (2022) - *Influence of a Landslide on a Tunnel in Loess-Bedrock Ground*. Applied Sciences, **12**(13): 6750. https://doi.org/10.3390/app12136750.

Tian X., Song Z. & Zhang Y. (2021) - *Monitoring and reinforcement of landslide induced by tunnel excavation: A case study from Xiamaixi tunnel*. Tunnelling and Underground Space Technology, **110**: 103796, https://doi.org/10.1016/j.tust.2020.103796.

Wei H., Wu D., Wu H., Tang L., Wang S. & Sun H. (2023) - *Coordinated evolution and mechanism characteristics of the tunnel-landslide system under rainfall conditions*. Engineering Failure Analysis, **146**: 107118. https://doi.org/10.1016/j.engfailanal.2023.107118.

Vlachopoulos N. & Diederichs M.S. (2009) - *Improved longitudinal displacement profiles for convergence confinement analysis of deep tunnels*. Rock Mech. & Rock Eng. **42**(2): 131-146.

Vlachopoulos N., Diederichs M.S., Marinos V. & Marinos. P. (2012) - *Tunnel behaviour associated with the weak Alpine rock masses of the Driskos Twin Tunnel system, Egnatia Odos Highway.* Can. Geotech. J., **50**: 1-30. dx.doi.org/10.1139/cgj-2012-0025.

Wu H. & Pai L. (2020) - *Research on the deformation mechanisms of a tunnel-landslide system based on the point safety factor of the interface*. E3S Web of Conferences **165**: 04068. https://doi.org/10.1051/e3sconf/202016504068.

Xiang B. & Liu E. (2021) - *Influence of excavation patterns on stress-deformation of landslide crossed orthogonally by tunnel association for computing machinery*. ACM ISBN 978-1-4503-8846-7/21/05. https://doi.org/10.1145/3475851.3475863.

Xiao J.Z., Dai F.C., Wei Y.Q., Min H., Chong X, Tu X.B. & Wang M.L. (2014) - *Cracking mechanism of secondary lining for a shallow and asymmetrically-loaded tunnel in loose deposits*. Tunnelling and Underground Space Technology, **43**: 232-240.

Xiao J.Z, Dai F. C., Wei Y. Q., Xing Y. C., Cai H. & Xu C. (2016) - *Comparative Analysis of Excavation Schemes for a Tunnel Constructed through Loose Deposits*. J. Perform. Constr. Facil., **30**(4): 04015061.

Zhang X., Krabbenhoft K. & Sheng D. (2015) - *Numerical simulation of a flow-like landslide using the particle finite element method*. J. Computational Mechanics, **55**(1): 167-177.

Zhang Y., Li J., Liu H., Li W., Li J. & Hou L. (2021a) - *Research on the Interaction Mechanism between Landslide and Tunnel Engineering*. Advances in Materials Science and Engineering, Volume 2021, Article ID 2265459, 14 pages https://doi.org/10.1155/2021/2265459.

ZhangY., Liu H., Li J., Huang Q., Ma X. & Li W. (2021b) - *Research on the mechanism of the influence of earthquake-induced landslides on the stress and deformation characteristics of tunnel*. Hindawi Advances in Materials Science and Engineering, Volume 2021, Article ID 3643100, 11 pages https://doi.org/10.1155/2021/3643100.

Zhang Y., Yang J. & Yang F. (2015) - *Field investigation and numerical analysis of landslide induced by tunneling.* Engineering Failure Analysis, **47**(A): 25-33.

Zhang Z., Zhao Q., Xu C. & Yang Y. (2017) - *Interaction analyses between tunnel and landslide in mountain area*. Journal of Mountain Science, **14**: (7): 1124-1139.

Zhijie S., Qingzhong K., Jie S., Yanchao W., Yi C. & Yamin L. (2020) - *The internal force numerical analysis of the tunnel structure affected by landslide-tunnel system*. 2nd Global Conference on Ecological Environment and Civil Engineering.

Zhou S., Tian Z., Di H., Gou P. & Fu L. (2020) - *Investigation of a loess-mudstone landslide and the induced structural damage in a high-speed railway tunnel*. Bull. Eng. Geol. Environ. **79**: 2201-2212, https://doi.org/10.1007/s10064-019-01711-y.

Zhu C., Yang F., Zheng J., Lin G. & Tian Z. (2021) - *Interaction and Treatment for Tunnels Orthogonally Traversing Large Bedrock Landslides*. KSCE J. Civ. Eng. **25**: 2758-2769, https://doi.org/10.1007/s12205-021-2231-y.

Zhu B., Lei M., Gong C., Zhao C., Zhang Y., Huang J., Jia C. & Shi C. (2022) - *Tunnelling-induced landslides: Trigging mechanism, field observations and mitigation measures*. Engineering Failure Analysis, **138**: 106387, https://doi.org/10.1016/j.engfailanal.2022.106387.

*Received November 2023 - Accepted March 2024*